INTENSITY DISTRIBUTION MODULATION OF MULTIPLE BEAM INTERFERENCE PATTERN

DOMINIKA JOCHCOVA, JAN KAUFMAN, PETR HAUSCHWITZ, JAN BRAJER, JAN VANDA

HiLASE centre, Institute of Physics of the Czech Academy of Sciences, Dolni Brezany, Czech Republic

DOI : 10.17973/MMSJ.2019_12_2019117

dominika.jochcova@hilase.cz

Nanostructuring and microstructuring approaches frequently used in microelectronics manufacturing, such as electron beam lithography or nanoimprint lithography, are considerably slow. In order to reduce processing time, laser patterning methods based on interference of multiple beams have been developed. Within one laser pulse, a significant part of an irradiated area on a sample surface is patterned with desired micro- or sub-microstructures. Nowadays, interference patterning goes beyond periodic lines and dots. Controlling the number of interfering beams, orientation of polarization vectors, relative phase shift, and the beam angle of incidence allows to customize the intensity distribution on the sample surface. Simulations of various interference patterns were calculated and verified on CMOS camera using 1030 nm laser diode. Based on these results, dot and line-like interference patterns were directly imprinted on the surface of carbon fiber reinforced polyether ether ketone plate by 1.8 ps, 11 mJ laser pulses at 1030 nm.

KEYWORDS

Direct Laser Interference Patterning, multiple beam interference, interference field simulation, Diffractive Optical Element, laser microstructuring

1 INTRODUCTION

Fabrication of micro patterns is desired in wide spectrum of applications, e.g. in optoelectronics where microstructured surfaces could increase efficiency of solar cells or organic light emitting diodes OLED [Lang 2016]. In addition, surfaces covered with periodic micropattern can exhibit new physical properties, such as hydrophobicity [Cardoso 2018] up to superhydrophobicity [Berger 2016] or hydrophilicity [Zhao 2015]. Microstructures can also enhance biocompatibility of body implants [Kurella 2005] reduce friction of components in automotive industry or generate antiadhesive properties of tools [Rosenkranz 2015]. The growing demand for more complex and refined shapes especially in metamaterials is a reasonable motivation to develop and upgrade techniques to affect intensity distribution within an interference field [Yang 2008], [Indrisiunas 2017]. The main capacity of this technology, however, remains in surface functionalization which requires less complex shapes, i.e., lines and dots.

In order to fabricate periodic microstructures, laser based methods and various fabrication approaches can be employed [Shaeffer 2012]. The most straightforward method is Direct Laser Writing (DLW) where the microstructure pattern is formed by scanning one laser beam across the specimen surface, processing one spot at a time. The laser beam can also be used to drill holes in a predetermined periodic configuration. This method requires considerable amount of time when compared to interference-based patterning methods [Morales 2018], [Lang 2016]. In Direct Laser Interference Patterning (DLIP) method, two or more coherent laser beams overlap to form an interference pattern which can be directly imprinted on the material surface. The material is ablated in all the interference maxima positions inside the interference area rather than just a single spot in DLW. That enables multiple spot irradiation within a single laser pulse. Moreover, subwavelength-sized patterns can be achieved when considering interference based methods.

This study deals with possibilities to modify interference pattern intensity distribution when beam parameters such as number of beams, relative phase shift, orientation of wave vectors in space and polarization are considered. Various arrangements of multiple beam interference were investigated using simulations in Wolfram Mathematica software and also experimentally with interference setup using CMOS camera.

2 THEORY OF MULTIPLE BEAM INTERFERENCE

Under specific circumstances, the laser light (i.e. electromagnetic radiation) can be approximated with an infinite monochromatic plane wave. Using a complex notation, the electric field modulation can be described as

$$\vec{E}_i(\vec{r},t) = \vec{E}_i(\vec{r}) \cdot e^{-i\omega t} = \vec{E}_0 e^{-i(\omega t - \vec{k}_i.\vec{r} + \varphi_i)} \quad (1)$$

where t denotes time coordinate, ω angular frequency, $\vec{r}$ position vector, $\vec{k}_i$ wave vector and φ_i denotes relative phase shift of i-th laser beam.

When the beams are conjoined, an interference phenomenon appears assuming the beams exhibit a significant degree of spacial and temporal coherence. For the simplest case of two beam interference, the distance between the interference maxima resp. minima Λ can be derived as

$$\Lambda = \frac{\lambda}{2\sin\theta} \quad (2)$$

where θ is the half angle between the beams and λ is the wavelength. This expression also determines limit for the smallest achievable structure that can be prepared. The theoretical limit is equal to λ/2 when θ equals to 90°.
When considering the superposition of plane waves, the final field is given by the sum of all contributions. A CMOS camera works as a quadratic detector and the intensity can be estimated within this formula when considering interference of two perfectly coherent beams with equal polarization and intensity:

$$I \sim 2\left|\vec{E}_0\right|(1+\cos(\vec{k}_1.\vec{r} - \vec{k}_2.\vec{r} + \varphi_1 - \varphi_2)) \quad (3)$$

General formula for multiple beams interference, where n is number of beams, is given by

$$I \sim \left|\vec{E}\right|^2 = \left|\sum_{i=1}^{n} \vec{E}_i\right|^2 = \sum_{i=1}^{n} \left|\vec{E}_{0i}\right|^2 + 2S \quad (4)$$

where *S* is denoted by

$$S = \sum_{j<i}^{n} \sum_{i=1}^{n} \vec{E}_{0i}.\vec{E}_{0j} \cos(\vec{k}_i.\vec{r} - \vec{k}_j.\vec{r} + \varphi_i - \varphi_j) \tag{5}$$

3 SIMULATION

4.1 Polarization and number of beams

When considering a multiple beam interference in general, the arrangement of wave and polarization vectors and overall symmetry is essential. Two examples of 12 beam interference are presented for comparison. The polarization vectors are arranged in radial symmetry with the following arrangements: A - each polarization vector lies in a plane defined by z axis and an appropriate wave vector and B - polarization vector is perpendicular to this plane. In both cases, the electric field vector oscillates in a plane perpendicular to the wave propagation direction. For graphics representation, see Fig. 1. The resultant intensity distribution is shown in Fig. 2. Narrow sharp maxima can be observed in case A, whereas case B exhibits a hollow maxima characteristic. Where sharp maxima are formed in case A, minima surrounded by blended maxima are formed in case B.

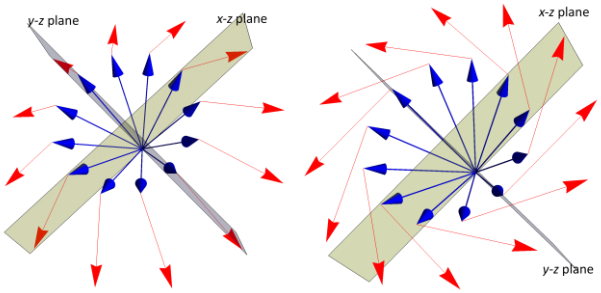

Figure 1: 3D scheme of geometry used in 12 beams interference arrangement. Blue arrows correspond to wave vectors and red arrows to appropriate vectors of polarization. On the left side, case A is depicted where each polarization vector lies in a plane defined by z-axis and an appropriate wave vector and on the right side, case B is shown where the all polarization vectors have the z-component equals to zero.

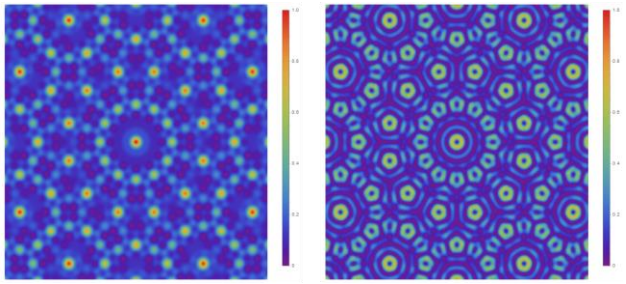

Figure 2: 12 beam interference field for two arrangement of polarization vectors with arrangement A on the left and arrangement B on the right. Intensity in the right image is rescaled to the left image. Maximal achievable intensity for the field on the right is 0.7 of maximal intensity obtained in the left image.

The number of interfering beams can affect sharpness of interference maxima. This phenomenon is investigated using net symmetry in 9 and 25 beam interference patterns. A net symmetry corresponds to an arrangement, where each wave vector lies on a line connecting a starting point, placed in z-axis (same for all wave vectors) and appropriate point in a symmetrical grid (this grid is perpendicular to the z-axis), see Fig. 3. The intensity distribution is shown in Fig. 4. Maximal intensity achieved in all simulations here presented is normalized to value of 1.

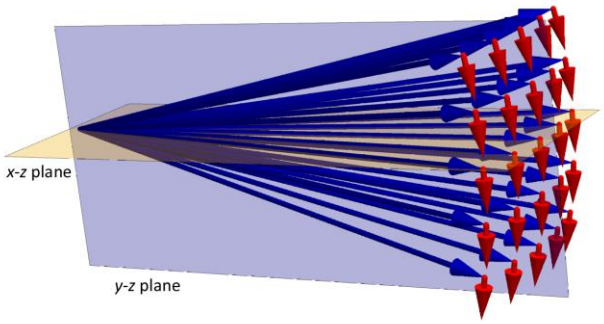

Figure 3: 3D scheme of 25 beams arranged in net symmetry. Blue arrows correspond to wave vectors and red arrows correspond to polarization vectors.

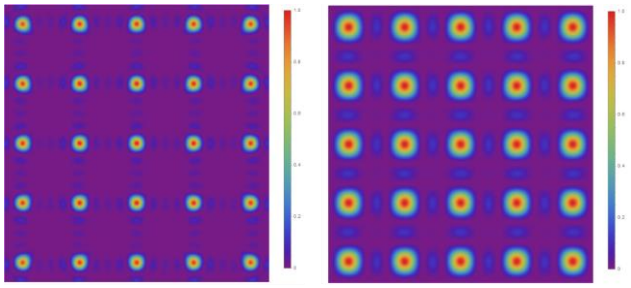

Figure 4: 25 beam interference (left picture) and 9 beam interference (right picture). Both arrangements obey a net symmetry and all polarization vectors have *x* component equals to zero. The demonstration shows that with increasing number of beams the interference pattern can be formed with much sharper maxima.

4.2 Phase shift

The sensitivity of the interference field to a relative phase shift of one beam has been investigated in four beam interference arrangement similarly to Fernandez [Fernandez 1998]. Considering incident angle θ equals to 60°, two configurations of polarization vectors are examined. In the first case C, all polarization vectors lie in a plane defined by z axis and appropriate wave vector. In the second case D, all polarization vectors have z component equals to zero. Changing the phase φ_1 causes the intensity distribution to vary and also maximal achievable contrast and visibility given by relation (6) is reduced (see Fig. 5).

Default polarization vector arrangement state C:

$$\vec{p}_1 = (1,0,0), \qquad \vec{p}_2 = (1,0,0),$$
$$\vec{p}_3 = \left(\frac{\sqrt{3}}{2}, 0, \frac{1}{2}\right), \qquad \vec{p}_4 = \left(\frac{\sqrt{3}}{2}, 0, -\frac{1}{2}\right).$$

Default polarization vector arrangement state D:

$$\vec{p}_1 = (1,0,0), \qquad \vec{p}_2 = (1,0,0),$$
$$\vec{p}_3 = (0,1,0), \qquad \vec{p}_4 = (0,1,0)$$

$$V = \frac{I_{MAX} - I_{MIN}}{I_{MAX} + I_{MIN}} \tag{6}$$

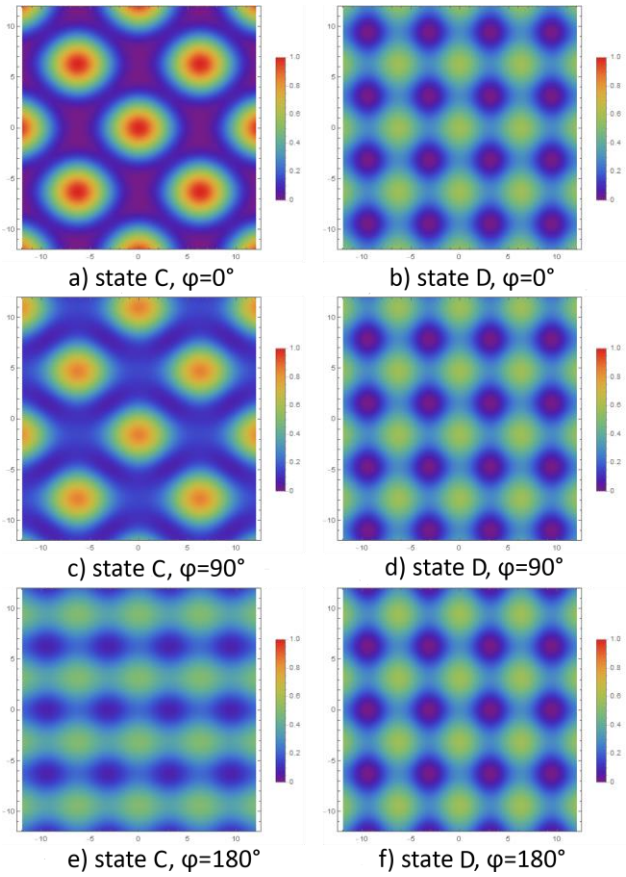

Figure 5: Interference field in phase shift varies from 0 to π. The left column corresponds to state C and the right column to state D. State C shows strong phase dependence and the intensity distribution changes both - in pattern and contrast whereas for case D, the pattern remains unchanged and moves among y-axis.

4.3 Polarization rotation

The sensitivity of four beam interference pattern to a polarization change is investigated within this chapter. Since the default polarization of all four beams is considered to be linear, the effect of rotation of several polarization vectors around appropriate wave vectors can be investigated (see Fig. 6). Rotation of polarization vector around appropriate wave vector causes changes in intensity distribution within the interference field. Sensitivity to this phenomenon is investigated in two arrangements C and D under the same conditions as in previous chapter. Polarization vector $\vec{p}_1$ is than rotated around wave vector $\vec{k}_1$ by angle Φ.

Default polarization vector arrangement state C:

$$\vec{p}_1 = (1,0,0), \qquad \vec{p}_2 = (1,0,0),$$

$$\vec{p}_3 = \left(\frac{\sqrt{3}}{2},0,\frac{1}{2}\right), \qquad \vec{p}_4 = \left(\frac{\sqrt{3}}{2},0,-\frac{1}{2}\right).$$

Default polarization vector arrangement state D:

$$\vec{p}_1 = (1,0,0), \qquad \vec{p}_2 = (1,0,0),$$

$$\vec{p}_3 = (0,1,0), \qquad \vec{p}_4 = (0,1,0)$$

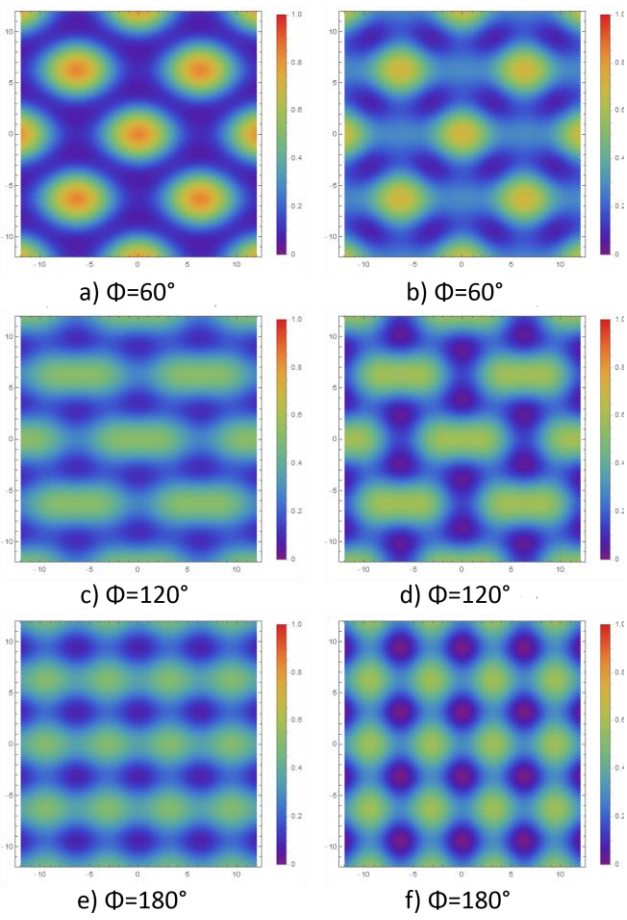

Figure 6: Sensitivity of an interference field to a polarization rotation of one beam. First column corresponds to state C, second column to state D. State C is 2π periodic with respect to Φ, state D is π periodic with respect to Φ.

4 EXPERIMENT

5.1 CW laser source

The interference setup shown in Fig. 7 easily allows to generate interference pattern using short pulse laser [Lasagni 2009], [Indrisiunas 2017]. Using this setup, differences between paths of individual beams are reduced and also sub-picosecond pulses can be overlapped in an interference area even though the pulses are less than 0.3 mm long in space. Diffractive Optical Element (DOE) was employed in order to split the initial beam into 4 beams equal in intensity, i.e., DOE's first order maxima. The beams are selected via an adjustable beam block which allows for 2, 3, 4 or 5 beam interference.

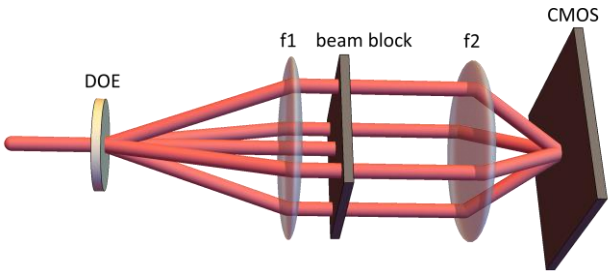

Figure 7: 3D interference setup scheme employing DOE with separation angle of 1.86° for λ=1030 nm.

The experiment was conducted using a continual wave laser diode operating at 1030 nm and a confocal imaging system with two lenses (f1=100 mm and f2=750 mm), both 50.8 cm in diameter. Since the distance between the lenses is equal to a sum of their focal lengths, the incoming collimated beam remains collimated after passing the system. The beam radius is enlarged by factor of f2/f1, i.e., 7.5. The intensity distribution of the interference field was detected via CMOS 1202 camera with pixel size of 5.3 µm. The smaller the θ, the bigger is the distance between interference maxima, resp. minima. The incident angle θ was set to approx. 1° in order to keep the distance between interference maxima significantly larger than the pixel size (see Fig. 8 and 9). The experiment was performed in a room temperature and under atmospheric pressure.

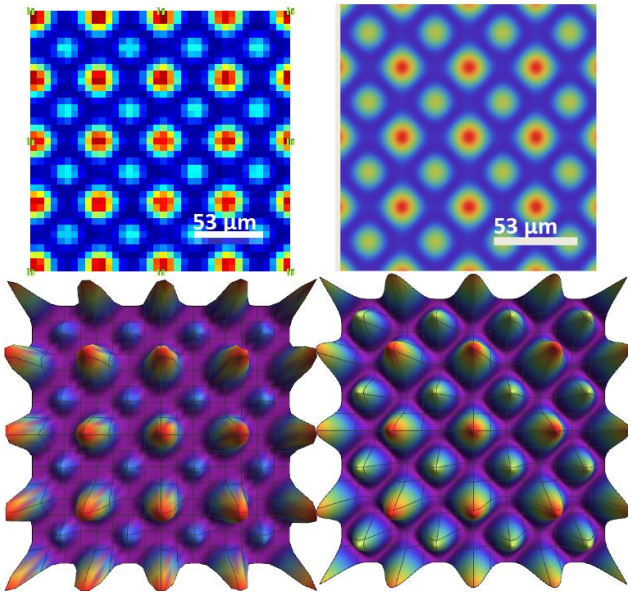

Figure 8: 5 beam interference pattern, comparison of 2D and 3D image obtained with CMOS camera with calculated interference intensity distribution via Wolfram Mathematica software.

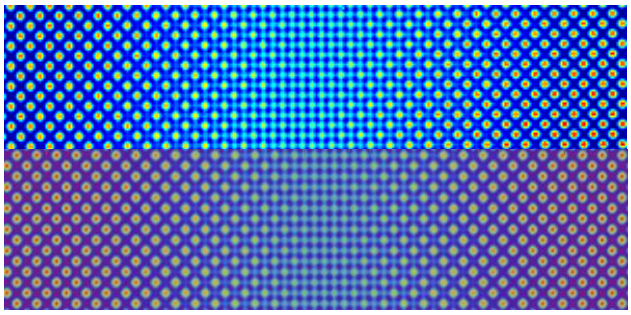

Figure 9: Pattern modulation in 4 beams interference intensity distribution. One of the beams is tilted i.e. comes at slightly different incident angle Θ than the others. This causes certain modulation in pattern to appear [El-Khoury 2018]. In this case it is caused by misalignment of the lens. Upper picture corresponds to a CMOS image, lower picture is appropriate simulation.

5.2 Sample processing

Dotted-like and line-like patterns were fabricated on a composite material CF-PEEK (Carbon Fiber reinforced Polyether Ether Ketone) using interference setup with DOE and convex lenses (f1=100 mm, f2=60 mm). Since the focal length of the f2 was smaller than the focal length of the lens f1, the beam radius was reduced by factor of 0.6. Beam parameters are shown in Tab. 1.

Laser processing parameters	
Wavelength, λ (nm)	1032
Energy per pulse, E (mJ)	Max 11
Repetition rate, f (Hz)	100
Pulse duration, t (ps)	1.8
Spot diameter, D (mm)	3
Number of interfering beams, n	3-5
Beam quality factor	<1.2

Table 1. Laser processing parameters

As a laser source, Perla system developed in HiLASE centre was employed. The pulse length in space was approximately 0.6 mm which means that a DOE-based setup that can be easily aligned is necessary in order to overlap the incident beams within the spatial coherence range. The energy losses on DOE and laser beam delivery system were 40%. When exposition time and energy per pulse increases, ablated areas i.e. dots get larger and more pronounced (see Fig. 10d.-e.).

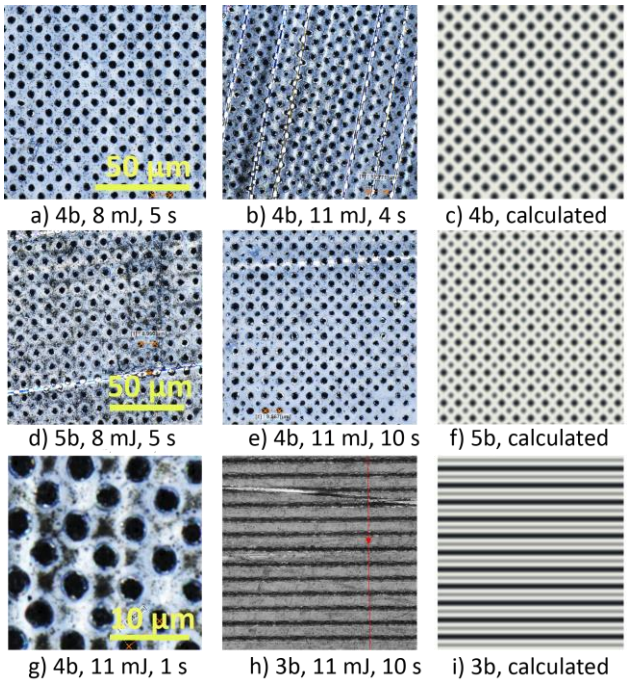

Figure 10: Confocal microscopic images of the treated CF-PEEK. 4b, 5b and 3b stands for 4, 5, 3 beam interference. The energy in the pulse follows and time stamp corresponds to the time of exposure. Second row corresponds to a five beam interference. The central less intensive maxima appear because of a contribution of the DOEs' zero order maximum.

The volume of treated area is approx. 3 mm in diameter. Since Gaussian beam is employed, only about 50% of the irradiated area is structured with desired dots, while the rest of the area is burnt, especially the central part. The fabricated pattern outside of the burn area corresponds well with the calculated pattern. The smallest distance between interference maxima achieved within the dotted-like pattern is 6.7 µm.

CONCLUSION

The ability to modify intensity distribution within an interference field by changing the relative phase shift of beams, polarization vectors, wave vectors orientation and number of beams was theoretically demonstrated via multiple simulations. By controlling the interference field, it is possible to customise

interference pattern for desired application, for example the fabrication of plasmonic metamaterials.

Some of the simulations of interference patterns were verified experimentally using DOE-based interference setup, first with continual laser diode operating at 1030 nm, and second, using ps laser source Perla, Direct Laser Interference Patterning method was employed in order to fabricate dotted-like and line-like pattern on the composite material of CF-PEEK. The smallest periodicity achieved in dotted-like pattern was 6.7 µm.

ACKNOWLEDGMENTS

The work is financially supported by the Ministry of Education, Youth and Sports of the Czech Republic (Programmes NPU I-Project no. LO1602 and Large Research Infrastructure Project No. LM2015086).

REFERENCES

[Berger 2016] Berger, J. et al. Controlling the optical performance of transparent conduction oxides using direct laser interference patterning. Elsevier, 2016, Vol.612., pp 342-349.

[Cardoso 2018] Cardoso, J.T. et al. Superhydrophobicity on hierarchical periodic surface structures fabricated via direct laser writing and direct laser interference patterning on aluminium. Optics and Lasers in Engineering, 2018, Vol.111., pp 193-200.

[El-Khoury 2018] El-Khoury, M. et al. Utilizing fundamental beam-mode shaping technique for top-hat Laser intensities in Direct Laser Interference Patterning. Journal of Laser Micro/Nanoengineering, 2018, Vol.13., No.3., pp 268-272.

[Fernandez 1998] Fernandez, A. and Phillion, D.W. Effects of phase shifts on four beam interference patterns. Appl. Opt., 1998, Vol.37., No.3., pp 473-478.

CONTACTS:

Bc. Dominika Jochcova
HiLASE centre
Za Radnici, Dolni Brezany, 252 41, Czech Republic
00420 605 784 108, dominika.jochcova@hilase.cz

[Indrisiunas 2017] Indrisiunas, S. et al. New opportunities for custom-shape patterning using polarization control in confocal laser beam interference setup. Journal of Laser Applications, 2017, Vol.29., No.1., pp 011501.

[Kurella 2005] Kurella, A. et al. Surface modification for bioiplants: the role of surface engineering. J. Biomater Appl. C, 2005, Vol.20., pp 5-50.

[Lang 2016] Lang, V. Et al. World record in high speed laser surface microstructuring of polymer and steel using direct laser interference patterning. In: Udo Klotzbach, Proceedings of the SPIE Conference Vol. 9736, San Diego, 4 March, 2016. Spiedigitallibrary, pp 97360Z-1-8.

[Lasagni 2009] Lasagni, A.F. et al. Periodic micropatterning of polyethylene glycol diacrylate hydrogel by laser interference lithography using nano and femtosecond pulsed lasers. Advanced Engineering Materials, 2009, Vol.11., No.3., pp 1438-1656.

[Morales 2018] Morales, A.I. et al. Micro-fabrication of high aspect ratio periodic structures on stainless steel by picosecond direct laser interference patterning. Journal of Materials Processing Technology, 2018, Vol.252., pp 313-321.

[Rosenkranz 2015] Rosenkranz, A. et al. Wear behavior of laser-patterned piston rings in squeeze film damper. Adv. Eng. Mater, 2015, Vol.17., pp 1208-1214.

[Yang 2008] Yang, Y. et al. Design and fabrication of diverse metamaterial structures by holographis litography. Opt. Express, 2008, Vol.16., pp 11275-11280.

[Zhao 2015] Zhao, L. et al. Antireflection silicon structures with hydrophobic property fabricated by three-beam laser interference. Applied Sufrace Sciences, 2015, Vol.346., pp 574-579.